Journal of Power Sources 209 (2012) 44–51

Contents lists available at SciVerse ScienceDirect

Journal of Power Sources

journal homepage: www.elsevier.com/locate/jpowsour

Nanostructured Co_3O_4 electrodes for supercapacitor applications from plasma spray technique

Raghavender Tummala, Ramesh K. Guduru*, Pravansu S. Mohanty

Department of Mechanical Engineering, University of Michigan, Dearborn, MI 48128, United States

ARTICLE INFO

Article history:
Received 9 November 2011
Received in revised form 19 February 2012
Accepted 20 February 2012
Available online 3 March 2012

Keywords:
Supercapacitors
Cobalt oxide
Pseudo capacitance
Solution precursor
Plasma deposition
Cyclability
Specific capacity

ABSTRACT

Among different transition metal oxides cobalt oxide (Co_3O_4) has attracted considerable attention for supercapacitor applications because of its superior electrochemical characteristics at relatively low cost. Nanostructured Co_3O_4 electrodes are usually prepared from powders using sol–gel and hydrothermal techniques, which require multi-step procedures and longer processing times. Here, we report synthesis and characterization of Co_3O_4 supercapacitor electrode films deposited directly on current collectors via a single step solution precursor plasma spray route. In this approach, an aqueous solution containing cobalt acetate is axially fed into plasma plume to produce nanoparticulates of Co_3O_4 via accelerated thermo-chemical conversion process, which are eventually deposited on a current collector substrate. Thus, developed Co_3O_4 electrodes showed nano particulate structure with porosity. The phase structure and crystallinity of Co_3O_4 electrode films were analyzed by X-ray diffraction and differential scanning calorimetry–thermogravimetry (DSC–TGA) studies. Electrochemical performance of these coatings showed a specific capacitance of ~162 F g^{-1} with a retention capacity of 72.2% after 1000 cycles for a specific current rate of 2.75 A g^{-1} in 6 M KOH electrolyte.

1. Introduction

Electrochemical supercapacitors are novel charge–storage devices with power density more than the batteries, and energy density more than the conventional capacitors [1–6]. They also exhibit excellent reversibility and longer cycle life compared to the batteries [3,5]. Supercapacitors are being employed in different applications ranging from mobile electronic devices to back-up power supplies, hybrid electric vehicles, etc. [1,5]. The energy storage mechanism in electrochemical capacitors is usually Faradic and non-Faradic in nature [3,5]. The non-Faradic capacitance arises from charge separation at the electrode/solution interface, whereas the Faradic pseudocapacitance comes from the reversible redox reactions occurring within the electroactive material because of several oxidation states. There are different metal oxides and metal hydroxides (e.g.: RuO_2, transition metal oxides, transition metal hydroxides, etc.) which can be used as supercapacitor electrodes [4,7,8]. RuO_2 is known to exhibit outstanding properties; however, due to the cost concerns considerable efforts have been shifted toward developing transition metals based (oxides and hydroxides) electrodes for supercapacitor applications. Among various transition metal oxides Co_3O_4 has attracted significant attention because of multiple applications, including in the batteries, catalysis and supercapacitors [4,9]. Also, Co_3O_4 was observed to exhibit good electrochemical performance in alkaline solutions with favorable pseudocapacitance characteristics [4]. Following redox reactions are considered to be responsible for pseudocapacitance of Co_3O_4 in the alkaline solutions [10]

$$CoOOH + OH^- \rightleftarrows CoO_2 + H_2O + e^- \quad (1)$$

$$Co_3O_4 + H_2O + OH^- \rightleftarrows 3CoOOH + e^- \quad (2)$$

Usually, nanostructured electrodes with porosity are desired for enhanced electrochemical reaction kinetics in supercapacitors as they provide large surface area, easy accessibility to the electrolyte and reduced mass and charge diffusion distances [4]. There has been extensive ongoing research to develop nanostructured Co_3O_4. Various processing techniques, including wet chemical processes [4,11–16], solid state syntheses [17], hydrothermal, electro deposition [18], RF magnetron sputtering [19] vapor based and microwave methods [20–24], have been adopted to tailor the structures of Co_3O_4 and thereby the electrochemical properties. But, most of these techniques lead to production of nanostructured powders of Co_3O_4, which consequently require further processing to develop the electrode coatings on the current collectors [25]. On the other hand, few research groups [26,14,27–36] have concentrated on developing self-supported nanowire/nanotube arrays of Co_3O_4 with or without template assistance. In contrast to these

* Corresponding author. Tel.: +1 313 583 6705; fax: +1 313 593 3851.
E-mail addresses: rkguduru@umich.edu, rameshkumarg5@yahoo.com (R.K. Guduru).

0378-7753/$ – see front matter © 2012 Elsevier B.V. All rights reserved.
doi:10.1016/j.jpowsour.2012.02.071

Fig. 1. Solution precursor plasma deposited flexible Co_3O_4 electrode on a stainless steel sheet (SS304) current collector.

techniques, here, we report rapid processing of nanostructured Co_3O_4 electrodes directly on a current collector using a solution precursor plasma deposition route. This approach makes use of an aqueous solution precursor comprising cobalt acetate to synthesize bulk scale, nanostructured, porous and flexible Co_3O_4 electrodes (see Fig. 1) in ambient conditions. It is also capable of developing electrode films/coatings on complex shapes. During the synthesis process, solution precursor is fed through an atomizer into the plasma plume, which then undergoes accelerated thermo-chemical conversion to form fine Co_3O_4 phase particulates. Thus, converted Co_3O_4 particles propel toward the substrate/current collector to form electrode films (thickness ~10–15 μm). Characterization of these electrodes in terms of microstructure and electrochemical performance are discussed in the forthcoming sections.

2. Experimental procedure

Solution precursor was prepared by dissolving 0.2 moles of cobalt acetate tetrahydrate (98% pure, Alfa Aesar, USA) in 1000 ml of deionized water. For complete dissolution of cobalt salt, solution was stirred for half an hour using a magnetic stirrer. A modified 100HE plasma gun (Progressive Technologies Inc., Grand Rapids, MI, USA) was used for depositing Co_3O_4 films on a 25 μm thick stainless steel (304 SS, McMaster Carr Inc., USA) sheet (current collector). An axial liquid atomizer was used to feed the solution precursor into the plasma plume. Spray parameters employed for deposition of Co_3O_4 films are shown in Table 1.

Table 1
Solution precursor plasma spray process parameters.

Parameter	Value
Power (kW)	55
Primary gas ($m^3\ h^{-1}$) (argon)	4.68
Secondary gas ($m^3\ h^{-1}$)	
Nitrogen and hydrogen	2.5 and 2.86
Standoff distance (mm)	135
Feed rate ($ml\ min^{-1}$) (solution precursor)	45
Material deposition density ($mg\ cm^{-2}$)	~2.9–3.8

Phase and crystallinity of all the materials were determined from X-ray diffraction (XRD) studies conducted using a Rigaku Miniflex X-ray diffraction machine with a Cu K_α radiation (λ = 1.5402 Å). DSC–TGA experiments were performed on SDT Q600 by heating the samples from room temperature to 1200 °C in air with a ramp rate of 20 °C min^{-1}. Surface and bulk microstructures were examined using SEM (Hitachi 2600-N) and TEM (Hitachi HT 7700), respectively. The samples for TEM studies were prepared following drop-cast method using scraped powders of Co_3O_4 films. Electrochemical characterization was done at room temperature using 6 M KOH electrolyte on Biologic VMP3 analyzer in three-electrode configuration, where Co_3O_4 electrode was the working electrode, a Ag/AgCl was the reference electrode, and a platinum mesh (2.5 cm × 2.5 cm) was the counter electrode. Electrochemical impedance spectroscopy measurements were done with a frequency range of 10 mHz–1 MHz.

3. Results and discussion

3.1. Synthesis and phase analysis

Fig. 2 shows a schematic of solution precursor plasma deposition technique used for the synthesis of Co_3O_4 electrodes in the present research. As shown in Fig. 2, the solution precursor is atomized by compressed air in the atomizer and enters into plasma

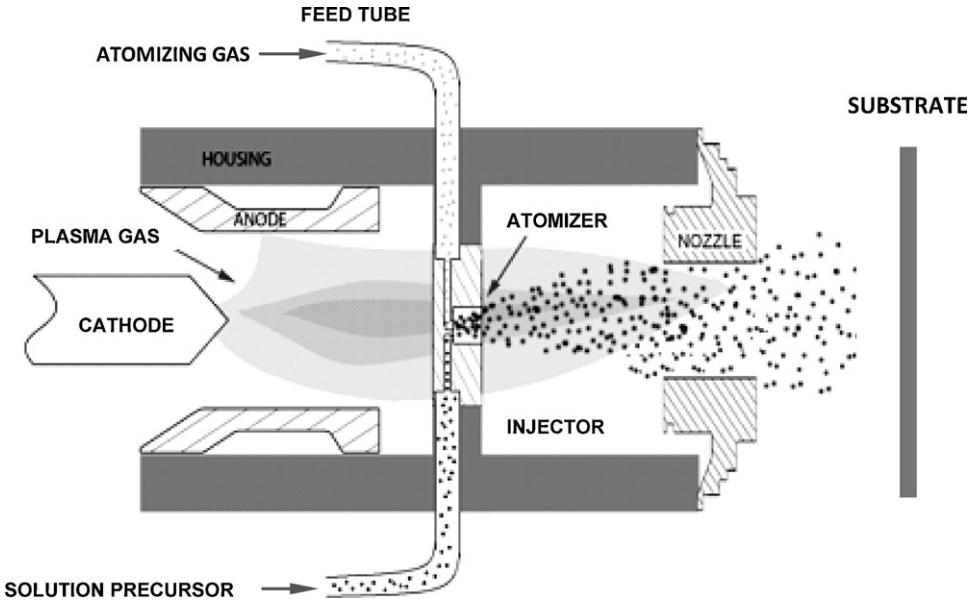

Fig. 2. Schematic of solution precursor plasma deposition technique.

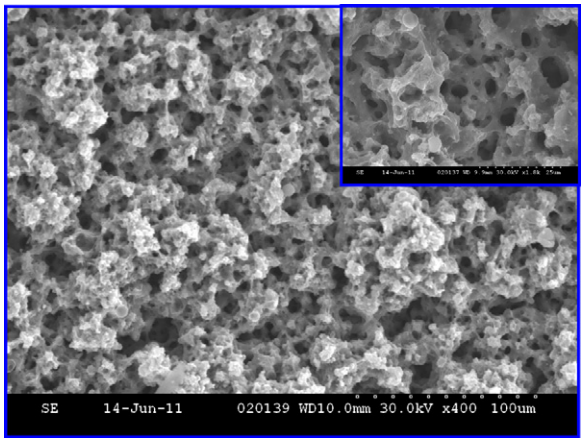

Fig. 3. Co_3O_4 electrode films synthesized using solution precursor plasma deposition technique (inset – zoom in view).

plume as fine droplets. Then the high temperatures of plasma plume accelerate the thermo-chemical conversion of the solution precursor droplets into Co_3O_4, which eventually deposit on the stainless steel (SS304) substrate i.e., current collector. Fig. 3 shows an SEM image of the Co_3O_4 electrode developed following this approach. Crystallinity and phase structure of the as-deposited films were determined by X-ray diffraction studies, which are shown in Fig. 4 along with the X-ray diffraction pattern of commercial Co_3O_4 powders. These studies confirm cubic phase and polycrystalline nature of the Co_3O_4 electrode films. It is evident from the literature [32,37,38] that formation of Co_3O_4 phase during thermo-chemical conversion of Cobalt acetate tetrahydrate (CATH) could be dependent on several factors; for example, the processing conditions employed. According to Mohamed et al. [32], dissociation of CATH at high temperatures (>400 °C), and especially in presence of air, can result in the formation of Co_3O_4 phase. Otherwise, it could lead to the formation of CoO or metallic Co phases in N_2 and H_2 atmospheres, respectively [37,38]. In the plasma deposition approach, the thermo-chemical conversion of solution precursor and deposition of the electrode films is usually carried out in ambient air, and therefore, influence of ambient oxygen on the formation of Co_3O_4 is quite plausible. However, the extent of thermo-chemical conversion of solution precursor droplets is dependent on several process parameters; such as the temperature of the plasma plume, size/mass of the atomized droplets, time of retention for the droplets within the plasma plume, and/or velocity

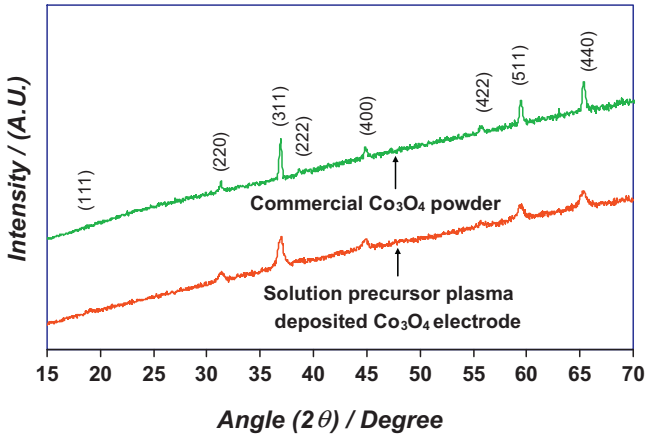

Fig. 4. X-ray diffraction patterns for solution precursor plasma deposited Co_3O_4 electrode and commercial Co_3O_4 powders.

of the droplet injection. In fact, all these parameters are interdependent, because the velocity of injection can limit the droplet size in thermo-chemical conversion process by affecting the total time of retention in the plasma plume. Small droplet size is preferred for rapid thermo-chemical conversion, and the size of the droplets during atomization process can be tailored by varying the pressure of compressed air as well as the flow rate of the solution precursor. But, the pressure of atomization gas (compressed air) can also act together with the velocity of the plasma jet and control the time of retention. Hence, these three parameters are very critical to achieve maximum conversion of the solution precursor before depositing on the substrate/charge collector. Detailed discussion of solution precursor spray deposition can be found elsewhere [39,40].

To understand the thermo-chemical conversion of solution precursor in the plasma plume, we conducted DSC–TGA studies on the solution precursor and these are shown in Fig. 5. The endothermic peak around 100 °C in DSC heat flow curve and associated weight loss in TGA data indicate evaporation of water molecules. However, further endothermic reaction above 100 °C with very little weight loss may be due to dissociation of CATH. Literature [32,37,38] suggests that dissociation of CATH occurs in different stages with increasing the temperature. Mohamed et al. [32] showed initial conversion of CATH into monohydrate and further dehydration with increasing temperatures above 200 °C. All the stages of dehydration are usually associated with very small amounts of weight loss and endothermic reactions. Although, the endothermic reactions in the present data are not clearly discernible in the DSC heat flow curve, but the TGA graph shows gradual weight loss due to the dehydration of CATH. According to Mohamed et al. [32] the volatile decomposition products of CATH were acetone, acetic acid, acetaldehyde and CO_2 and the exothermic peak around 360 °C could be because of the oxidation of non-volatile dissociation products, such as formation of Co_3O_4 phase. However, with further increase in the temperature there was an endothermic peak around 900 °C and it must be due to conversion of Co_3O_4 into CoO with a slight amount of oxygen loss, which is also apparent from the weight loss in TGA curve. Therefore, we believe that the solution precursor will undergo similar thermo-chemical conversion process when the atomized droplets of solution precursor are exposed to the plasma plume, but at rapid rates because of high temperatures of the plasma (~10,000–12,000 °C). In the early stages of conversion process, a huge volume change in the size of solution precursor droplets can also be expected due to evaporation of water molecules. But, as the particles exit the plasma plume and propel toward the substrate in the ambient atmosphere, their temperatures fall rapidly. The temperature of the substrate was measured to be around 350–365 °C throughout the deposition process, which is below 900 °C and because of this reason we expect conversion of CoO back into Co_3O_4 in the deposited coatings. On the other hand, it is also possible that the size of some of the droplets could also limit the high temperature conversion of Co_3O_4 into CoO in the plasma plume itself because of large thermal mass. The other possibilities could include incomplete conversion of the solution precursor droplets (in the plasma plume), and incomplete back conversion of CoO into Co_3O_4 due to rapid quenching after exiting the plasma plume. Therefore, one can expect to have Co_3O_4 phase in the as-deposited coatings along with a mixture of partially converted solution precursor phase (CATH), as well as quenched CoO phase. In the present study, the X-ray diffraction pattern of as-deposited Co_3O_4 film (see Fig. 4) did not indicate existence of CoO or unconverted CATH phases. Therefore, to determine the existence of other phases and the thermal stability of the Co_3O_4 films, DSC–TGA scans were run on scraped powders of as-deposited films, which are shown in Fig. 6. The DSC heat flow curve shows endothermic nature in the beginning with couple of exothermic peaks above 200 °C. There is also a continuous weight loss till 400 °C in the TGA

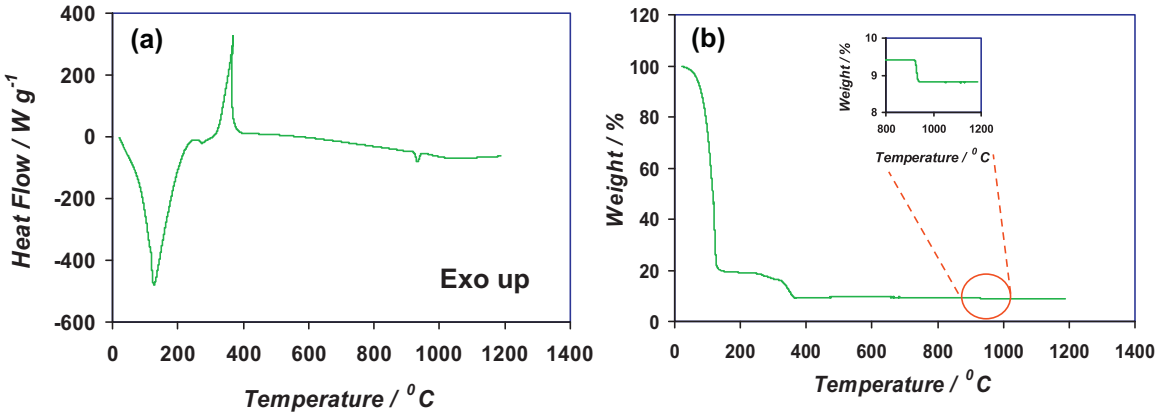

Fig. 5. Differential scanning calorimtery (DSC)–thermogravimetry (TGA) analysis of solution precursor (a) DSC – heat flow curve and (b) TGA – weight change curve.

curve. The endothermic behavior and corresponding weight loss could be attributed to possible evaporation of adsorbed moisture in the coatings. However, the exothermic peaks and weight loss above 200 °C, which is similar to the DSC–TGA curves shown by the solution precursor, indicate presence of unconverted material in the coatings. Absence of X-ray diffraction peaks for unconverted material in Fig. 4 may be related to the detection limit of the X-ray diffraction technique. Above 400 °C, there is no change in weight till 900 °C. The endothermic peak and corresponding weight loss around 900 °C could be attributed to conversion of Co_3O_4 into CoO. Thus, these studies clearly indicate a requirement for controlled optimization of plasma deposition process parameters to obtain full conversion of the solution precursor into Co_3O_4 phase.

3.2. Microstructural characterization

The surface microstructures of as-deposited Co_3O_4 films are shown in Fig. 3 at different magnifications. During the deposition process, the thermo-chemically converted particles in the plasma plume could melt partially/fully and fuse together into clusters because of very high temperatures of the plasma plume, and therefore, films could have agglomerates of fused particles. Due to the particulate nature, these films also exhibit porosity as shown in Fig. 3. Usually, porosity of the electrode material provides large surface area and an easy access for the electrolyte, and thereby facilitates redox reactions during charge/discharge process. Therefore, porous microstructures of the current Co_3O_4 electrodes are very much desired for enhanced performance of supercapacitors. Fig. 7 shows the bulk microstructural analysis of Co_3O_4 films. Fig. 7(a) shows a high magnification TEM image of agglomerates of Co_3O_4 particulates, and these particulates must have been the resultant of thermo-chemical conversion of the solution precursor droplets. The size of these particles is in the range of 10–50 nm. Nanoparticles of the Co_3O_4 phase are also very important for better electrochemical performance as they provide large surface area with reduced mass and charge diffusion distances for rapid electrochemical reactions. Fig. 7(b) shows interplanar spacing between two consecutive (1 1 1) planes of Co_3O_4 crystal structure inside a particulate. The diffraction pattern in the inset of Fig. 7(a) and high-resolution image in Fig. 7(b) also confirm the cubic phase of Co_3O_4.

3.3. Electrochemical characterization

Electrochemical characterization of the as-deposited Co_3O_4 electrode films was done without adding binder or carbon additive.

3.3.1. Cyclic voltammograms

The cyclic voltammetry (CV) studies were performed between −0.1 and 0.5 V at different scan rates, which are shown in Fig. 8. Non-Faradic capacitance is usually known to be independent of the scan rates and the potentials employed, as well as symmetry of the CV scans is expected with respect to the zero current line. However, the scan rate dependent behavior and asymmetry of the CV scans shown in Fig. 8 apparently indicate Faradic reactions and a consequence of ohmic resistance as a result of electrolyte diffusion within the electrode, which are the typical characteristics of pseudocapacitance behavior [3]. At slow scan rate ($2\,mV\,s^{-1}$) the redox peaks are well defined at 0.37 V (anodic) and 0.267 V (cathodic) and literature suggests that these potentials could be the resultant of redox transitions of Co^{3+}/Co^{4+} [10,41] following the electrochemical reaction shown in Eq. (2). At high scan rates (above

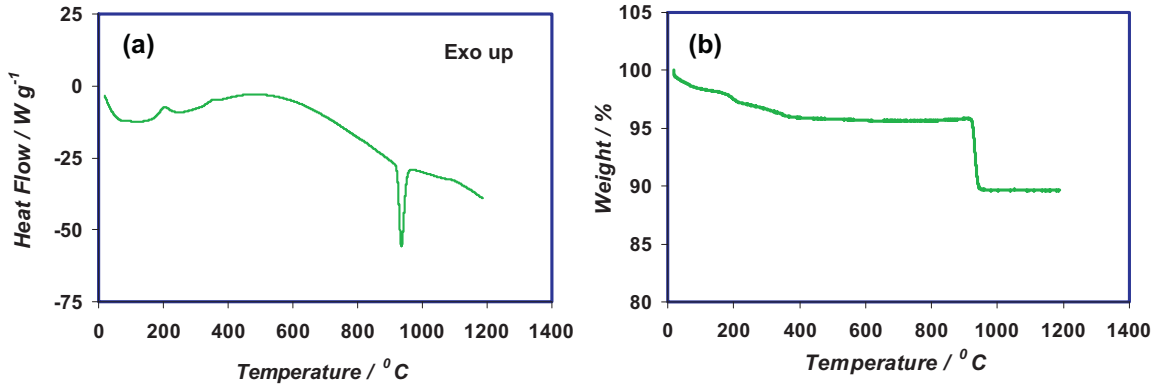

Fig. 6. Differential scanning calorimtery (DSC)–thermogravimetry (TGA) analysis of solution precursor plasma deposited Co_3O_4 electrode films.

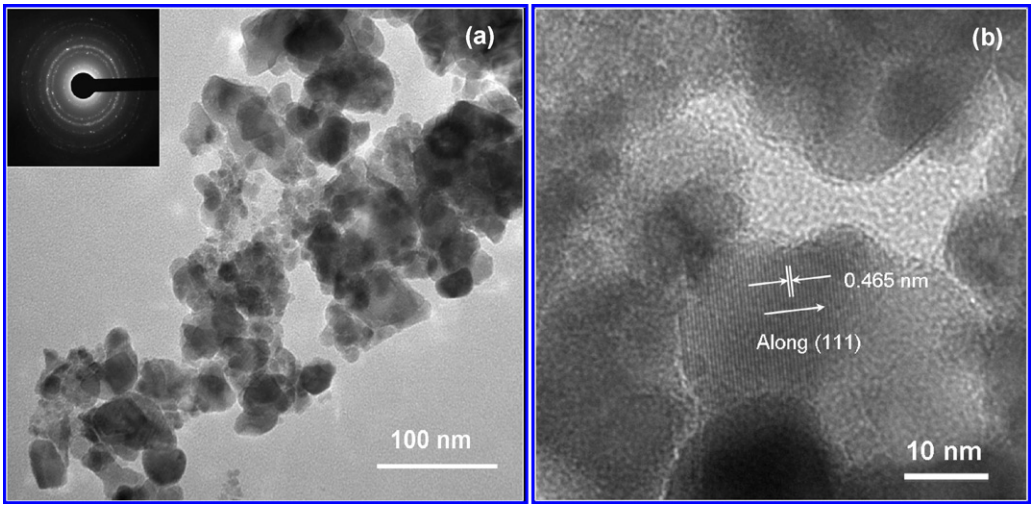

Fig. 7. Transmission electron microscopy images of Co_3O_4 electrode film – (a) particulates of Co_3O_4 phase and the diffraction pattern is shown in the inset, and (b) high resolution lattice image of Co_3O_4 particulates.

5 mV s^{-1}) one anodic peak and two cathodic peaks could be seen in Fig. 8. According to Cui et al. [41] the anodic and corresponding cathodic peaks should be at 0.34 V/0.13 V and 0.4 V/0.25 V for Co^{2+}/Co^{3+} (corresponding to Eq. (1)) and Co^{3+}/Co^{4+} (corresponding to Eq. (2)) redox transitions, respectively. At a scan rate of 2 mV s^{-1}, there were only one anodic and cathodic peaks present in the CV scan; however, the second cathodic peak started to appear only when the scan rate was 10 mV s^{-1} or higher. But the anodic peaks were shifted to 0.44 V or above for the scan rates 10 mV s^{-1} or higher. Also, the anodic peak voltages for the above redox reactions are very close enough to overlap. Therefore, we believe that absence of the second peak could be either due to broad nature of the anodic peaks in Fig. 8 at all the scan rates, or due to shift of the anodic peaks toward higher potentials (>0.5 V) at higher scan rates (>10 mV s^{-1}). The shift in the anodic peak toward higher potentials, and the cathodic peaks toward lower potentials with increasing the scan rates could be related to the conductivity and thereby possible polarization of the electrodes. At high scan rates, some of the active surfaces on the electrode may not be accessible; also absence of carbon or conductive additives may lead to localized polarization of the electrodes [34,35]. The relation between the scan rate and cathodic peak current for Co^{4+}/Co^{3+} transition is shown in Fig. 9. A linear relationship between the square root of the scan rate and the peak current indicates that the reaction kinetics followed during the redox reactions may be controlled by diffusion process.

3.3.2. *Electrochemical impedance spectroscopy and galvanostatic charge–discharge analysis*

Fig. 10 shows the Nyquist plot for impedance of the Co_3O_4 electrode before cycling for 1000 galvanostatic charge–discharge cycles at a rate of 2.75 A g^{-1}. The impedance plot shows a semicircle in the high frequency region and a straight line in the low frequency region. The point of intersection on real axis in the high frequency region (~2.5 Ω) indicates internal resistance of the electrode in an open circuit condition. Usually this resistance is due to combination of ionic resistance of the electrolyte, intrinsic resistance of the active material, and contact resistance between the active material and current collector [42]. High impedance of the present electrodes could be attributed to several reasons, such as absence of carbon or conductive additives in the electrode, porous nature of the active material, and also possible residual stresses in the active material. During the plasma spray process, rapid cooling of the deposited material can usually result in residual stresses in the as deposited Co_3O_4 films. The semicircle in the high frequency

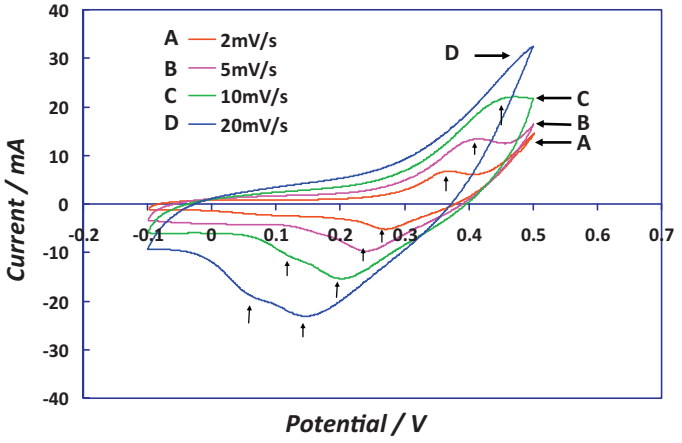

Fig. 8. Cyclic voltammograms (CVs) of solution precursor plasma deposited Co_3O_4 electrode films scanned at different rates.

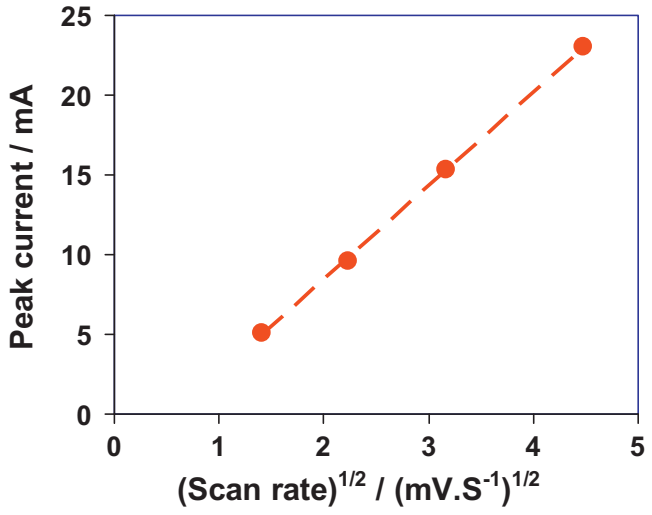

Fig. 9. Relation between the cathodic peak current in the CV scans shown in Fig. 8 for a redox transition of Co^{4+}/Co^{3+} and the CV scan rates.

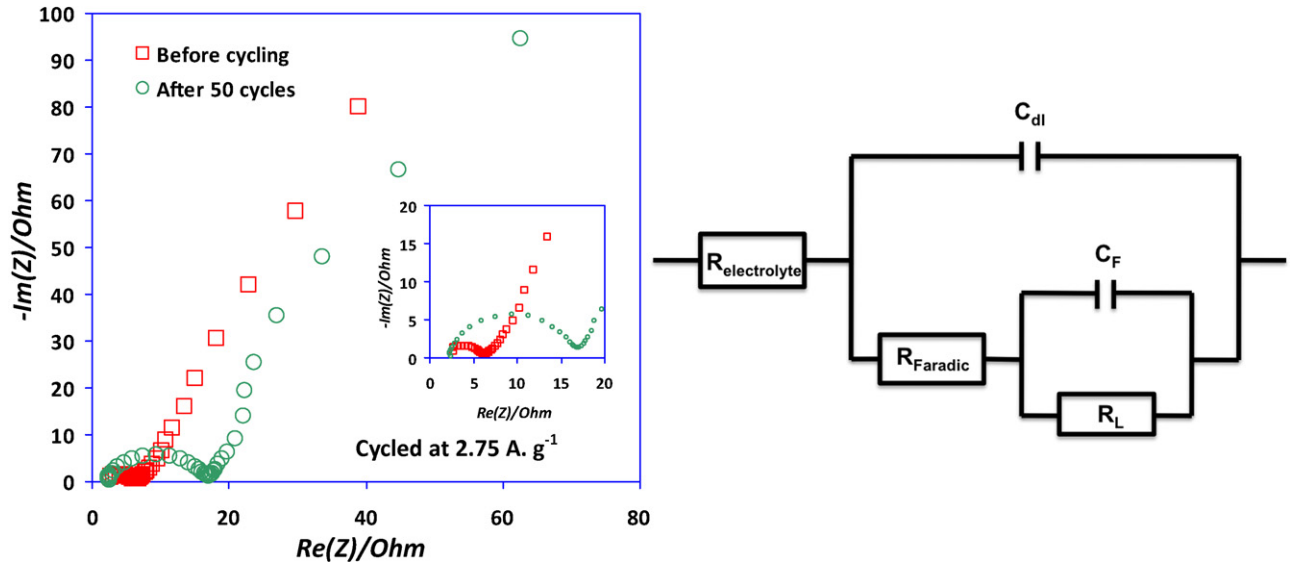

Fig. 10. (a) Electrochemical impedance spectroscopy of the solution precursor plasma deposited Co_3O_4 electrode films before galvanostatic charge–discharge cycling as well as after 50 charge–discharge cycles at a specific current rate of 2.75 A g^{-1}, (b) Equivalent circuit model used to fit the impedance spectroscopy data.

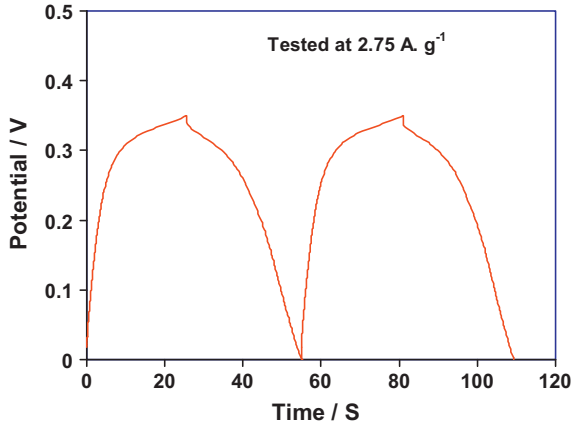

Fig. 11. Galvanostatic charge–discharge cycles of the solution precursor plasma deposited Co_3O_4 electrode films tested at a specific current rate of 2.75 A g^{-1}.

region is due to Faradic reactions at the electrolyte and electrode interface during the charge transfer process. The linear part of the impedance spectrum after the semicircle, which is also called Warburg impedance, is related to the diffusion process of the electrolyte within the pores and surface layers of the electrode. The linear part of the impedance is also typical characteristic of the capacitive behavior [2,3,5]. Fig. 10(b) shows the equivalent circuit model used to fit the impedance spectrum shown in Fig. 10(a) with different elements (also see Table 2). It is apparent that the value of pseudocapacitance element is more than the double layer capacitance element indicating more of the pseudocapacitance behavior of the present Co_3O_4 electrode films.

Fig. 11 shows the first two galvanostatic charge–discharge cycles for the Co_3O_4 electrode tested at a rate of 2.75 A g^{-1}. The drop in potential during the discharge process can be attributed to the internal resistance of the electrode. The specific capacitance of was calculated from the following equation

$$C = \frac{I \times \Delta t}{\Delta V \times m} \quad (3)$$

where C is (F g^{-1}) is the specific capacitance, I (A) is the galvanostatic current employed during charge/discharge cycles, m (g) is the amount of active material, Δt (s) is the time elapsed for charge/discharge cycles, and ΔV(V) is the potential interval chosen for charge/discharge process. The charge/discharge cycles in Fig. 11 showed columbic efficiency close to ~99.5%, which indicates excellent reversibility of the electrodes during charge–discharge process and this could be attributed to the porosity and nanostructures of the active material as they provide large surface area with reduced charge and mass diffusion distances along with easy accessibility to the electrolyte.

Fig. 12 shows the specific discharge capacitance of the Co_3O_4 electrode tested for 1000 charge/discharge cycles. It is apparent from Fig. 12 that there is a decrease in the specific capacitance with increasing the number of cycles. A total capacity of 72.2% was retained after the 1000th discharge cycle. From Fig. 10 also it is clear that there is an increase in the impedance with increasing the number of cycles. Although the impedance curves for the Co_3O_4 electrode show no change in the internal resistance before cycling and after 50 cycles, but there is an increase in the impedance in the semicircle and Warburgh regions, which is related to charge transfer phenomenon in the electrode. The elements of the equivalent circuit model (see Fig. 10(b)) fitted to both the impedance spectra (before cycling and after 50 cycles) showed in Table 2 indicate negligible changes in the electrolyte resistance and double layer capacitance (C_{dl}) values, however a considerable increase in the faradic resistance (also, see the increased diameter of the semicircle). In addition, slightly reduced pseudocapacitance (C_F) element

Table 2
EIS parameters from the equivalent circuit for solution plasma sprayed Co_3O_4 electrode.

	$R_{electrolyte}$ (Ω cm^2)	$R_{Faradic}$ (Ω cm^2)	C_{dl} (mF cm^{-2})	C_F (mF cm^{-2})	R_L (Ω cm^2)	χ^2
Before cycling	2.25	5.241	0.313	40.7	6.89×10^{14}	0.0787
After 50 cycles	2.51	14.68	0.0547	36.1	1289	0.0838

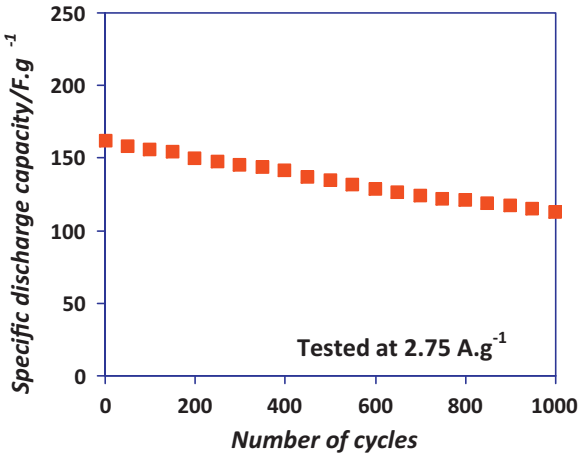

Fig. 12. Specific discharge capacity of the solution precursor plasma deposited Co_3O_4 electrode films tested for 1000 cycles at a specific current rate of 2.75 A g^{-1}.

also indicates overall reduced capacitance of the films with more leakage. Therefore, decrease in capacitance with increasing number of cycles could be likely because of the increased impedance, and the reason for increased impedance could be due to fatigue of the active material during cycling. Pseudocapacitance can lead to fatigue of the electrode material during the Faradic redox reactions because of the diffusion of ionic species into the active material following Frumkin isotherm [2,3,8]. Hence the supercapacitors, similar to batteries, can suffer from lack of stability and cyclability, and this can be explained in the present case with absence of binder and carbon additives, which usually provide cushioning effect during cycling. But, it is less severe in capacitors compared to the batteries because of the surface layer adsorption of ions. However, addition of carbon and relieving of stresses in the as-deposited films by preheating the charge collector may help improve the cyclability of the electrodes.

We also tested the Co_3O_4 electrodes at different specific current rates to understand the discharge characteristics as well as determine the capacity. Fig. 13 shows the discharge curves at different specific current rates along with an inset showing the variation of capacitance as a function of the specific current rates. It is clear that with increasing the discharge rates, the specific capacitance decreased and this is likely due to resistance as well as the extent

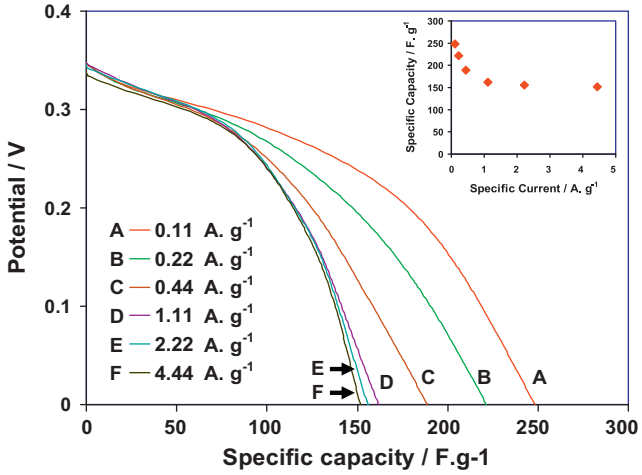

Fig. 13. Galvanostatic charge–discharge cycles of the solution precursor plasma deposited Co_3O_4 electrode films tested at different specific current rates (inset – specific discharge capacity as a function of specific current).

of utilization of the electrodes. At high discharge rates, the potential drop will increase during the discharge process and thereby reduce the overall capacity of the electrode. On the other hand, increased currents can also lead to insufficient Faradic redox reactions and thereby reduce the extent of utilization of the active material for capacitance [34].

4. Summary

In summary, we have demonstrated successful processing of nanostructured Co_3O_4 electrodes directly on charge collectors with an industrial scale solution precursor plasma deposition technique. DSC–TGA, X-ray diffraction and TEM examination confirm the cubic Co_3O_4 phase in the as-deposited material. However, optimization of plasma deposition in terms of atomization and a close temperature control of the process are required for a complete conversion of the solution precursor into Co_3O_4 phase. Electrochemical characterization indicated that the specific discharge capacities of solution precursor plasma deposited Co_3O_4 electrodes could be highly reversible. Cyclability data reveals that continuous charge/discharge cycling process may lead to fatigue of the material with lack of cushioning effect, and thus result in an increase in the impedance as well as reduced capacity because of the Faradic nature of the capacitance. Therefore, addition of carbon along with optimization of plasma deposition may be helpful to obtain long-term cyclability.

References

[1] P. Simon, Y. Gogotsi, Nature 7 (2008) 845.
[2] B.E. Conway, Electrochemical Supercapacitor Scientific Fundamentals and Technological Applications, Kluwer, 1999.
[3] B.E. Conway, J. Electrochem. Soc. 138 (1991) 1539.
[4] G. Wang, L. Zhang, J. Zhang, Chem. Soc. Rev. (2011), doi:10.1039/C1CS15060J.
[5] R. Kotz, M. Carlen, Electrochim. Acta 45 (2000) 2483.
[6] Y. Zhang, H. Feng, X. Wu, L. Wang, A. Zhang, T. Xia, H. Dong, X. Li, L. Zhang, Int. J. Hydrogen Energy 34 (2009) 4889.
[7] S. Saranagapani, B.V. Tilak, C.P. Chen, J. Electrochem. Soc. 143 (1996) 3791.
[8] S. Trasatti, P. Kurzweil, Platinum Met. Rev. 38 (1994) 46.
[9] M. Stanley Whittingham, Chem. Rev. 104 (2004) 4271.
[10] C. Barbero, G.A. Planes, M.C. Miras, Electrochem. Commun. 3 (2001) 113.
[11] L. Gomez Camer, F. Martin, J. Morales, L. Sanchez, J. Electrochem. Soc. 155 (2008) A189.
[12] X.W. Lou., D. Deng, J.Y. Lee, J. Feng, L.A. Archer, Adv. Mater. 20 (2008) 258.
[13] F. Zhan., B. Geng, Y. Guo, Chem. Eur. J. 15 (2009) 6169.
[14] W.Y. Li., L.N. Xu, J. Chen, Adv. Funct. Mater. 15 (2005) 851.
[15] F. Tao., C. Gao, Z. Wen, Q. Wang, J. Li, Z. Xu, J. Solid State Chem. 182 (2009) 1055.
[16] J.S. Do., C.H. Weng, J. Power Sources 146 (2005) 482.
[17] Y.M. Kang., K.T. Kim, J.H. Kim, H.S. Kim, P.S. Lee, J.Y. Lee, H.K. Liu, S.X. Dou, J. Power Sources 133 (2004) 252.
[18] S. Lichušina, A. Chodosovskaja, A. Selskis, K. Leinartas, P. Miečinskas, E. Juzeliūnas, Chemija (2008) 19.
[19] H.K. Kim, T.Y. Seong, J.H. Lim, W.I. Cho, Y.S. Yoon, J. Power Sources 102 (2001) 167.
[20] W. Yao., J. Yang, J. Wang, Y. Nuli, J. Electrochem. Soc. 155 (2008) A903.
[21] H. Zhang., J. Wu, C. Zhai, X. Ma, N. Du, J. Tu, D. Yang, Nanotechnology 19 (2008) 035711.
[22] Y. Liu., C. Mi, L. Su, X. Zhang, Electrochim. Acta 53 (2008) 2507.
[23] J. Jiang., J. Liu, R. Ding, X. Ji, Y. Hu, X. Li, A. Hu, F. Wu, Z. Zhu, X. Huang, J. Phys. Chem. C 114 (2010) 929.
[24] Y. Lu., Y. Wang, Y. Zou, Z. Jiao, B. Zhao, Y. He, M. Wu, Electrochem. Commun. 12 (2010) 101.
[25] Linda Gaines, Roy Cuenca. Available from: www.transportation.anl.gov/pdfs/TA/149.pdf, 2000.
[26] C.K. Chan, H. Peng, G. Liu, K. McIlwrath, X.F. Zhang, R.A. Huggins, Nat. Nanotechnol. 3 (2008) 31.
[27] F. Li., Q.Q. Zou, Y.Y. Xia, J. Power Sources 177 (2008) 546.
[28] Yanguang Li, Bing Tan, Yiying Wu, Nano Lett. 8 (1) (2008) 265.
[29] G. Che., B.B. Lakshmi, E.R. Fisher, C.R. Martin, Nature 393 (1998) 346.
[30] P.L. Taberna., S. Mitra, P. Poizot, P. Simon, J.M. Tarascon, Nat. Mater. 5 (2006) 567.
[31] C.R. Sides., C.R. Martin, Adv. Mater. 17 (2005) 125.
[32] M.A. Mohamed, S.A. Halawy, M.M. Ebrahim, J. Therm. Anal. 41 (1994) 387.
[33] Robin W. Grimes, Andrew N. Fitch, J. Mater. Chem. 1 (3) (1991) 461.

[34] X. Qing, S. Liu, K. Huang, K. Lv, Y. Yang, Z. Lu, D. Fang, X. Liang, Electrochim. Acta 56 (2011) 4985.
[35] Y. Li, B. Tan, Y. Wu, J. Am. Chem. Soc. 128 (44) (2006) 14258.
[36] L. Gong, X. Liu, L. Su, L. Wang, J. Solid State Electrochem. (2011), doi:10.1007/s10008-011-1327-6.
[37] R.W. Grimes, A.N. Fitch, J. Mater. Chem. 1 (3) (1991) 461.
[38] T. Wanjun, C. Donghua, Chem. Pap. 61 (4) (2007) 329.
[39] J. Karthikeyan, C.C. Berndt, J. Tikkanen, J.Y. Wang, A.H. King, H. Herman, Nanostruct. Mater. 9 (1997) 137.
[40] L. Xie, X. Ma, E.H. Jordan, N.P. Padture, D.T. Xiao, M. Gell, Mater. Sci. Eng. A 362 (2003) 204.
[41] L. Cui, J. Li, X.-G. Zhang, J. Appl. Electrochem. 39 (2009) 1871.
[42] J. Xu, L. Gao, J. Cao, W. Wang, Z. Chen, Electrochim. Acta 56 (2010) 732.